applied sciences

MDPI

Article

Research on Online Monitoring of Partial Discharge of Insulation Defects in Air Switchgear Based on Characteristic Gases

Yi Tian *, Haotian Niu, Shuai Wang and Guixin Zhu

School of Electronics and Information, Xi'an Polytechnic University, Xi'an 710048, China; niuhaotian@stu.xpu.edu.cn (H.N.); 210411025@stu.xpu.edu.cn (S.W.); 13398468594@163.com (G.Z.)
* Correspondence: tianyi@xpu.edu.cn

Abstract: Air switchgear is an important power equipment in the transmission, transformation, and distribution process of the power system. Insulation defects can lead to partial discharge, which is one of the primary causes of air switchgear failure. Current monitoring methods primarily rely on detecting ultra-high frequency or ultrasonic signals generated by partial discharge to identify insulation defects. However, these methods are prone to external signal interference, resulting in substantial detection errors. Based on gas discharge theory and engineering practice, this paper uses three typical defects to represent the main insulation defects of air switchgear, namely metal protrusion defects, insulation layer air gap defects, and metal particle defects. After that, the validity of the numerical model to describe the partial discharge process of air switchgear insulation defects is verified by the volt-ampere characteristic curve. The discharge process of three typical defect models was investigated by using the numerical model, and the variation curves of the volume fractions of CO, NO_2, and O_3 gases at different voltage levels and different discharge durations were obtained. After analysis, the volume fractions of the three characteristic gases are unique under different defect models and partial discharge quantities. Finally, this paper designed a partial discharge inversion method based on characteristic gases, and fitted time-domain regression equations and partial discharge inversion regression equations based on the changes in volume fractions of the three characteristic gases measured. The research results of this paper provide a theoretical basis for online detection of partial discharge in high-voltage air switchgear through characteristic gases. The method proposed in this paper can also be applied to other gas-insulated equipment, such as GIS, metal-enclosed switchgear, and vacuum circuit breakers.

Keywords: air switchgear; insulation defects; characteristic gases

check for updates

Academic Editors: Ernst Gockenbach and Gerard Ghibaudo

Received: 16 May 2024
Revised: 10 November 2024
Accepted: 25 December 2024
Published: 26 February 2025

Citation: Tian, Y.; Niu, H.; Wang, S.; Zhu, G. Research on Online Monitoring of Partial Discharge of Insulation Defects in Air Switchgear Based on Characteristic Gases. *Appl. Sci.* **2025**, *15*, 2538. https://doi.org/10.3390/app15052538

Copyright: © 2025 by the authors. Licensee MDPI, Basel, Switzerland. This article is an open access article distributed under the terms and conditions of the Creative Commons Attribution (CC BY) license (https://creativecommons.org/licenses/by/4.0/).

1. Introduction

In the process of power generation, transmission, distribution, and energy conversion in the power system, high-voltage air switchgear is used for opening, closing, controlling, and protecting electrical equipment, with a working voltage level mainly between 10–35 kV. However, throughout the manufacturing, transportation, and operational maintenance phases of the switchgear, scratches and metal fragments may accumulate within the cabinet due to improper handling. Due to different coefficients of expansion and aging of materials inside the switchgear, air gaps may occur in the components. The above defects will deteriorate the original insulation conditions of the air switchgear, change the electric field distribution, and lead to partial discharge, which will cause serious safety accidents [1,2].

When partial discharge occurs, various signals can be detected in the surrounding area, such as electrical, ultrasonic, and electromagnetic signals [3–6]. For these signals generated by partial discharge, they can be obtained through pulse current method, ultrasonic detection method, and UHF detection method [7–14]. The analysis methods for detecting signals mainly include spectrogram method, wavelet transform method, compressed sensing method, and phase-diagram-based analysis method [15,16]. These methods are indirect measurements, and their accuracy is easily affected by external interference. Furthermore, the classification of sources that cause partial discharge still needs further improvement.

The gas inside the air switchgear is composed of 78% N_2, 21% O_2, and 1% other gases. When the electric field strength inside the air switchgear reaches the critical electric field strength, charged particles acquire sufficient kinetic energy in the electric field, collide with other neutral particles, and ionize. When these particles collide, some new gas is produced. Detecting these newly generated gases can determine whether partial discharge has occurred. By analyzing the volume fraction and rate of change of the detected characteristic gases, the discharge situation of partial discharge can be evaluated. The gas composition analysis method is used to detect characteristic gases, and its working environment has little impact on the detection results. The commonly used methods for detecting gas composition are dedicated sensor method and ultraviolet and gas chromatography method [17,18].

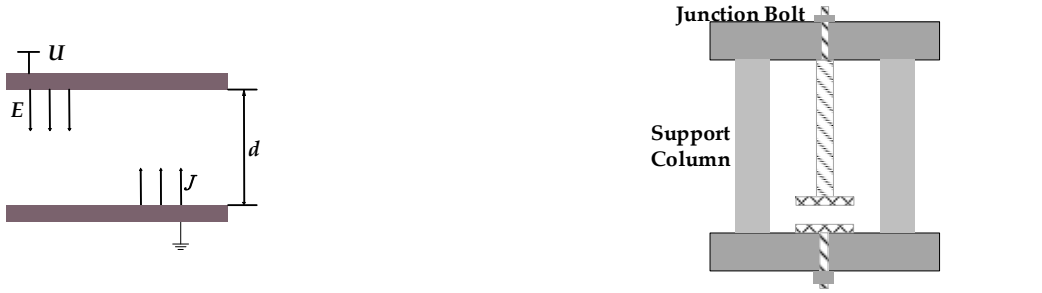
In recent years, the study of characteristic gases generated by partial discharge in switchgear has attracted considerable attention. The decomposition components of switchgear partial discharge characteristics are studied [19]. Materials Studio was used to simulate and calculate all possible components generated during the air discharge process. The generation process of each component gas is analyzed, and it explains the reasons why characteristic gases cause insulation defects in air switchgear. A characteristic gas concentration detection system based on the characteristic gases generated by partial discharge is designed, and the distribution of derived gases is determined using the FLUENT fluid dynamics research platform, providing a theoretical basis for the optimized layout of the characteristic gas detection system [20]. The simulation model of defect construction during atmospheric pressure gas discharge processes has been studied [21,22]. The volt-ampere characteristic curves of insulation defects at both ends during partial discharge were measured and compared with the volt-ampere characteristics output by the simulation model, thus verifying the accuracy of the constructed simulation model.

The characteristic gas method is to detect one or more characteristic gases, which is a chemical detection method, so it will not be affected by the same kind of interference signal in the surrounding environment. When the power equipment partially discharges, air, as an insulating medium, will decompose composite and other chemical reactions, resulting in new gases. By detecting and analyzing these newly generated gases, the current partial discharge situation of the power equipment can be obtained. Based on the above analysis, this paper proposes the use of characteristic gas method to detect partial discharge of insulation defects in air switchgear. Firstly, a numerical model and experimental platform were established to simulate the partial discharge process of insulation defects in air switchgear based on the mechanism of air discharge. Secondly, this paper verifies the effectiveness of the numerical model in describing the partial discharge process of insulation defects in air switchgear through the volt-ampere characteristic curve. Finally, numerical models were used to study the discharge process of three typical defect models, and the change curves of CO, NO_2, and O_3 gas volume fractions at different voltage levels and discharge durations were obtained. The inversion relationship between the change of characteristic gas volume fraction and the development of partial discharge was established. This paper lays a theoretical foundation for the design of online monitoring of partial discharge in insulation defects of air switchgear based on characteristic gases.

2. Test Model

2.1. Gap Discharge

Based on the characteristics of air gap insulation defects in air switchgear, this paper selects a plate-plate electrode with a distance of d between two parallel plate electrodes to simulate air gap discharge defects. Apply voltage $\boldsymbol{U}$ to the high electrode side of the plate-plate electrode, ground the low voltage side, and set the initial temperature of the simulation area to 300 K and the air pressure to 101.3 kPa. The pole plate is made of stainless-steel electrode with 0.1~0.4% carbon content. The plate electrode is simulated in a cylindrical shape with a diameter of 45 mm and a height of 25 mm. There is a gap of 1 mm for the electrode plates. The simulation model of air gap insulation discharge is shown in Figure 1, where $\boldsymbol{E}$ is the electric field, the lines with arrows next to them are the electric field lines, and $\boldsymbol{J}$ is the current, described. The experimental design model of air gap insulation discharge is shown in Figure 1.



(**a**) Simulation model of gap insulation defects. (**b**) Experimental model of gap insulation defects.

Figure 1. The model of gap insulation defects.

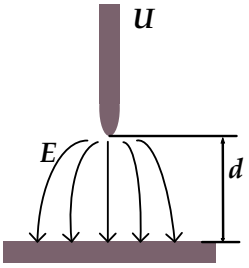
2.2. Metal Protrusion Discharge

In the process of switchgear manufacturing, transportation, operation, and maintenance, metal protrusions are more likely to be generated, so metal protrusion defects are a common type of discharge. The simulation model of metal protrusion insulation defects is shown in Figure 2. To facilitate the study of the mechanism of partial discharge caused by metal protrusion defects and the influence of discharge on the volume fraction of characteristic gases, this paper chooses to use needle-plate electrodes to simulate discharge defects based on the characteristics of metal protrusion insulation defects in air switchgear. The needle electrode is connected to the high voltage source, and the plate electrode is grounded. The pole plate is made of a stainless-steel electrode with 0.1~0.4% carbon content. The plate electrode simulates the grounding housing of a switchgear and uses a stainless-steel electrode with a radius of 60 mm and a thickness of 10 mm, the surface of which is polished. The needle-plate spacing is set to 10 mm. The tip has an approximate radius of curvature of 0.3 mm and a 30° cone angle. The experimental design model of a metal protrusion insulation defect is shown in Figure 2.

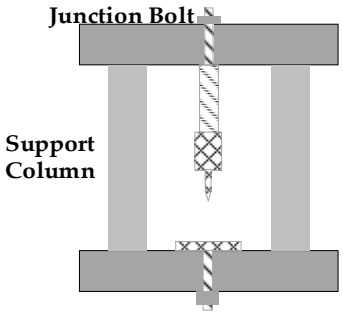
2.3. Metal Particle Discharge

In this paper, the bowl-ball electrode is chosen to simulate metal particle discharge defects in air switchgear insulation based on their specific characteristics. Metal particles are subject to electrostatic force F_e, gravity F_g, and Lorentz force F_L, in order for metal particles in the switchgear cabinet to get the force situation shown in Figure 3, where $\boldsymbol{H}$ is the magnetic field, the alternating magnetic field produced by the alternating current. This paper uses a bowl ball electrode with a ball electrode connected to high voltage and a bowl-shaped electrode connected to ground, and the ball electrode and bowl-shaped electrode are concentric. Use 1000 mesh sandpaper and aluminum plate friction to obtain

metal particles, select metal particles of similar size, and sprinkle them in the center of the bowl-shaped electrode. The bowl electrode is a grounding electrode with a radius of 60 mm. The ball electrode is a high-voltage electrode with a radius of 22 mm. The experimental design model of metal particle insulation defect is shown in Figure 3.

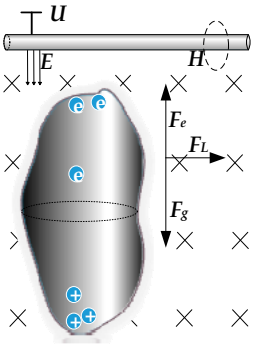


(**a**) Simulation model of metal protrusion.

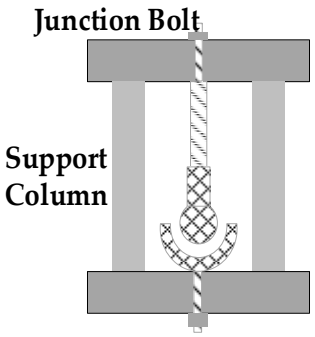


(**b**) Experimental model of metal protrusion.

Figure 2. The model of metal protrusion.



(**a**) Analysis of forces on metal particles.



(**b**) Experimental model of bowl ball electrode.

Figure 3. The model of metal particle defects.

2.4. Test Platforms

The partial discharge test device consists of an AC power supply, insulation defect model, coupling capacitor, partial discharge tester, oscilloscope, and other parts. The insulation defects are in the atmospheric environment. A coupling capacitor provides a pathway for high-frequency signals, ensuring the transmission of high-frequency currents. The high-voltage electrode of the insulation defect model is connected to the coupling capacitor, and the low-voltage side is well grounded. The partial discharge tester is connected to the other end of the coupling capacitor. The discharge of the insulation defect causes the transfer of charge from the coupling capacitor. The partial discharge tester detects the amount of partial discharge from this process. The function of the impedance box is to convert the current coupled to the measurement circuit into a voltage value. The partial discharge meter measures the voltage value on the impedance box to the current value, and thus obtains the amount of partial discharge. The oscilloscope detects the change of voltage and current in this process. The partial discharge test setup is shown in Figure 4. In the measurement of characteristic gases generated by insulation defect discharge, CO and NO_2 are measured using the flue gas analyzer (RBR ecom-EN2), and O_3 is measured using the online ozone analyzer (NICON GDT-550). Through on-site experiments, it was found that the characteristic gases CO, NO_2, and O_3 molecules rapidly and uniformly distribute throughout the entire space under the influence of thermal motion.

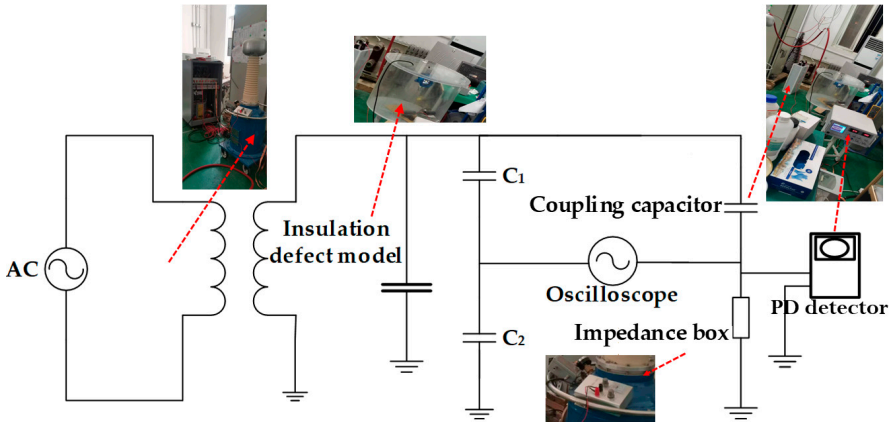


Figure 4. Partial discharge test platforms.

3. Numerical Model

3.1. Governing Equation

The governing equations include the equation describing the continuity of various particles, the Poisson equation describing the distribution of the electric field, and the equation for the conservation of the electron energy density. In addition, charged particles are subjected to an electric field force in an electric field, the force equation of which is shown in Equation (1).

$$M\frac{dv}{dt} = eE \tag{1}$$

where M is the electron mass, v is the electron velocity, and eE is the force on the electron in the electric field E.

The initial position equation of the stressed particle is shown in Equation (2).

$$\begin{aligned} z &= z_0 + (z_1 - z_0)R_f \\ r &= r_0 + (r_1 - r_0)R_f \end{aligned} \tag{2}$$

where R_f is a random number in [0, 1].

The force, initial position, and initial velocity of the particle are known and can be found for any moment and any position. The velocity and relative position of the ion at the nth time step are shown in Equations (3) and (4). The chemical reaction equations used in this paper are referenced in the literature.

$$v_n = v_{n-1} + (em/M)\Delta t \tag{3}$$

$$x_n = x_{n-1} + v_{n-1}\Delta t + (\frac{em}{2M})(\Delta t)^2 \tag{4}$$

where v_n is the particle velocity of the layer at time n; v_{n-1} is the particle velocity of the layer at time $n-1$; x_n is the particle position of the layer at time n; and x_{n-1} is the particle position of the layer at time $n-1$.

3.2. Validation of the Numerical Model

The flow chart of the partial discharge test and simulated volt-ampere characteristic curve measurement for insulation defects in air switchgear is shown in Figure 5.

The system for testing and simulating insulation defects and partial discharge, constructed in this paper, investigates the discharge current of insulation defects when subjected to a sine cycle (20 ms) power supply voltage. During the experiment, the ambient temperature was 300 K and the atmospheric pressure was 0.1 MPa. The discharge current is tested using the HIOKI CT6701 current probe (Hioki E.E. Corporation, Nagano, Japan).

The time-varying characteristic curves of current and voltage for experimental testing and numerical simulation are shown in Figure 6. From Figure 6, it can be observed that the simulated current calculated by the numerical model has the same trend as the experimental current. During the rising period of the positive half axis of the input voltage, the discharge current first remains constant, and then rapidly increases in the opposite direction to the voltage direction. During the falling period when the input voltage reaches the positive half axis, the discharge current reverses. This phenomenon indicates that in a discharge cycle, it can be essentially divided into two discharges of opposite polarity. During the rise of the negative half axis of the input voltage, the discharge current first remains constant and then rapidly increases in the opposite direction to the voltage direction. The time interval between two discharges of the positive and negative half axes of the input voltage is 1 ns~2 ns.

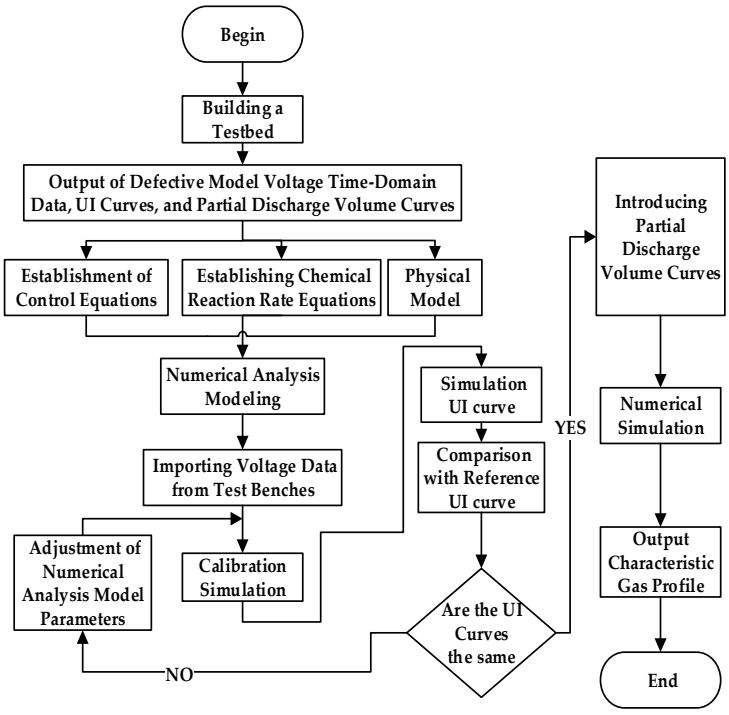


Figure 5. Flow chart of volt-ampere characteristic curve measurement.

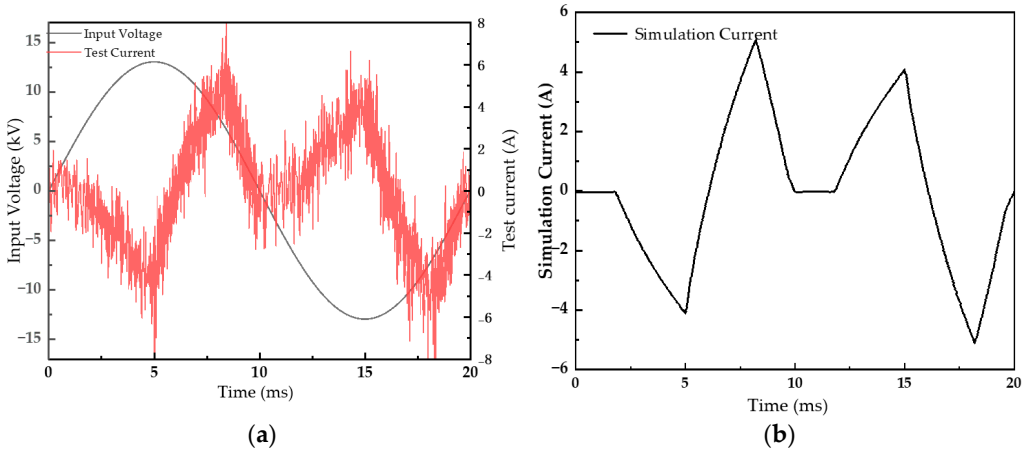


Figure 6. Discharge current characteristic curves of test and simulation platform. (**a**) Voltage and discharge current. (**b**) Discharge current of the simulation platform.

4. Characterization of the Discharge of Insulation Defects in Switchgear

In partial discharge monitoring, the magnitude of partial discharge is influenced by various factors. To ensure that the partial discharge generated by different insulation defects is only affected by a single variable in this paper, the types of insulation defects are constantly changing during experiments and simulations, while other influencing factors such as surrounding environment, electrode voltage, and insulation defect location remain consistent. In this paper, partial discharge is used as a parameter to describe the severity of insulation defects in air switchgear, and the measurement of characteristic gases indirectly reflects the magnitude of partial discharge. The partial discharge volume was tested on the testing platform shown in Figure 4.

4.1. Characterization of Characteristic Gases Generated by Metal Protrusion Discharge

4.1.1. Variable Properties of Characteristic Gases in Metal Protrusion Discharge

(1) Characterization of the change in volume fraction of CO

The characteristic curves of the volume fraction of CO with time after the voltage of 11 kV, 13 kV, 15 kV, and 17 kV are applied to the metal protrusion defects are shown in Figure 7. The pathway for CO production under metal protrusion defects is that the air contains a small amount of CO_2, which is ionized and converted to CO when the discharge occurs.

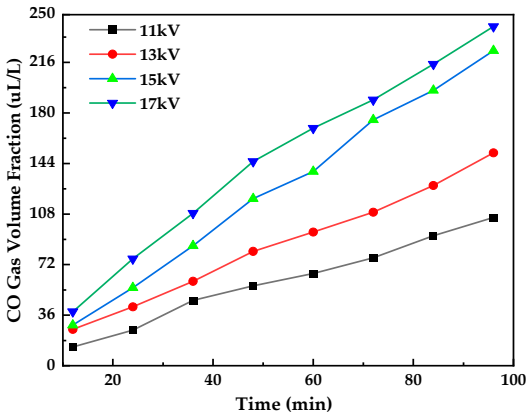


Figure 7. CO gas volume fraction variation curve.

(2) Volume fraction change characteristics of NO_2

The volume fraction of NO_2 in the 11 kV, 13 kV, 15 kV, and 17 kV voltages to the metal protrusion defects, change with the time characteristic curve shown in Figure 8.

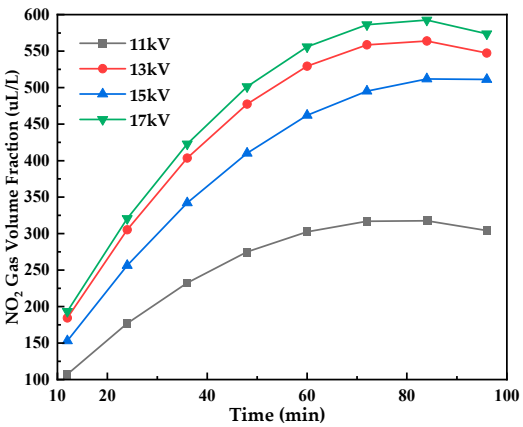


Figure 8. NO_2 gas volume fraction of air gap defects.

The generation of NO_2 under the defect of metal protrusion includes two pathways. First, N_2 collides with O particles and generates NO_2 by chemical reaction. Second, the high-energy particles composing the plasma are generated by a collision breaking the N-N bond of the N element, and NO_2 is generated by the compounding of N and O. The strong oxidizing gases oxidize NO to substances with higher nitrogen content ratios, such as NO_2, NO_3, and N_2O_5. Once the reaction attains dynamic equilibrium, the volume fraction of different gas components becomes locally saturated and stable.

(3) O_3 volume fraction change characteristics

The O_3 volume fraction in the 11 kV, 13 kV, 15 kV, and 17 kV voltages to the metal protrusion defects, and the characteristic curve with the time change, are shown in Figure 9.

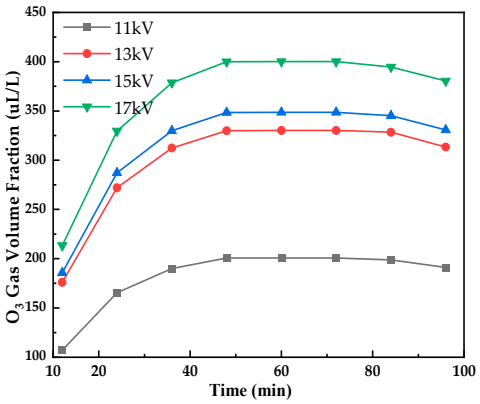


Figure 9. The O_3 gas volume fraction of gap discharge.

The O element in NO_2 under metal protrusion defects originates from the decomposition of O_2 into O element under the action of energetic particles. From Figure 9, it can be seen that the O_3 gas volume fraction experiences rapid growth before 40 min and tends to stabilize after 40 min. The reason for this is that reducing gases in the air (e.g., CO) limit the growth of O_3.

4.1.2. Relationship Between Characteristic Gases and Discharge Volume in Metal Protrusion Discharge

The changes in CO, NO_2, and O_3 characteristic gases generated during partial discharge of metal protrusion defects were tested using the constructed switchgear insulation defect partial discharge characteristic gas testing platform. The characteristic curves of the relationship between the production of characteristic gases CO, NO_2, and O_3 during different discharge times and the partial discharge amount are shown in Figure 10.

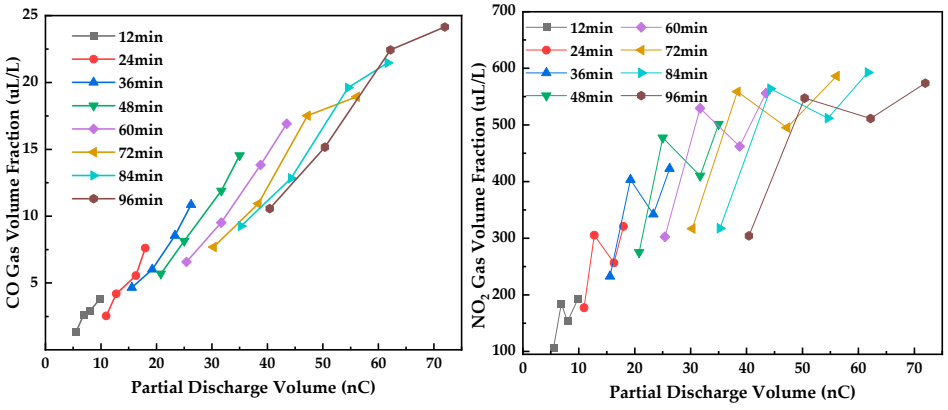
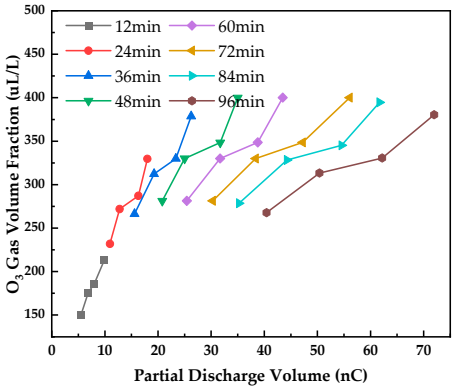


Figure 10. *Cont.*



(c)

Figure 10. Variation curves of gas volume fractions of CO, NO_2, and O_3 with partial discharge volume caused by metal protrusions. (**a**) Variation curve of CO volume fraction with partial discharge volume. (**b**) Variation curve of NO_2 volume fraction with partial discharge volume. (**c**) Variation curve of O_3 volume fraction with partial discharge volume.

Based on Figure 10, it is evident that CO and O_3 gas volume fractions exhibit a linear increase trend with the increase in partial discharge, whereas NO_2 initially increases linearly with the increase in partial discharge but later tends to saturate.

4.1.3. Regression Equation of Characteristic Gas Volume Fraction and Discharge Volume in Metal Protrusion Discharge

To study the effect of the partial discharge of switchgear air gap defects on the characteristic gas, this paper introduces a regression equation to fit the partial discharge and gas volume fraction into a one-variable quadratic equation, which is shown in Equation (5).

$$\varphi = ax^2 + bx + c \tag{5}$$

where φ is the O_3 gas volume fraction; x is the partial discharge; a, b, and c are the coefficients of the quadratic term, the coefficients of the primary term, and the constant term of the regression equation, respectively. The 95% confidence interval for the overall mean is calculated as shown in Equation (5).

The regression equation for the volume fractions of CO, NO_2, and O_3 was found as shown in the following equation:

$$y = 0.273766x_{CO} + 2.84508 \tag{6}$$

$$y = 8.73874e^{-5}x_{NO_2}^2 + 0.03904x_{NO_2} + 1.40024 \tag{7}$$

$$y = 1.42644e^{-4}x_{O_3}^2 + 0.11887x_{O_3} - 18.92568 \tag{8}$$

where x_{CO}, x_{NO_2}, x_{O_3} represents the volume fractions of CO, NO_2, and O_3 when the magnitude of partial discharge is y.

The characteristic gases generated under different partial discharge amounts within a certain period of time (here 24 h) were fitted, and Figure 11 was obtained. Figure 11 shows the regression equation, 95% confidence interval, and 95% prediction space for partial discharge volume.

4.2. Characteristics of Characteristic Gases Generated by Gap Discharge

4.2.1. Variable Properties of Characteristic Gases in Gap Discharge

(1) Characterization of the Change in Volume Fraction of CO

The graph of the change of the volume fraction of CO gas is shown in Figure 12. There is a growing trend in CO gas volume fraction as the discharge duration increases and the

degree of gas ionization increases. In addition, the growth trend of CO gas volume fraction is also affected by the voltage level. The higher the voltage level, the greater the degree of ionization of the gas in the discharge interval, and the volume fraction of CO gas will also increase. At lower voltage levels, the change in the volume fraction of CO gas shows a linear increase. After the voltage is increased, the curve of the volume fraction of CO gas first grows linearly, and then there is a saturation trend.

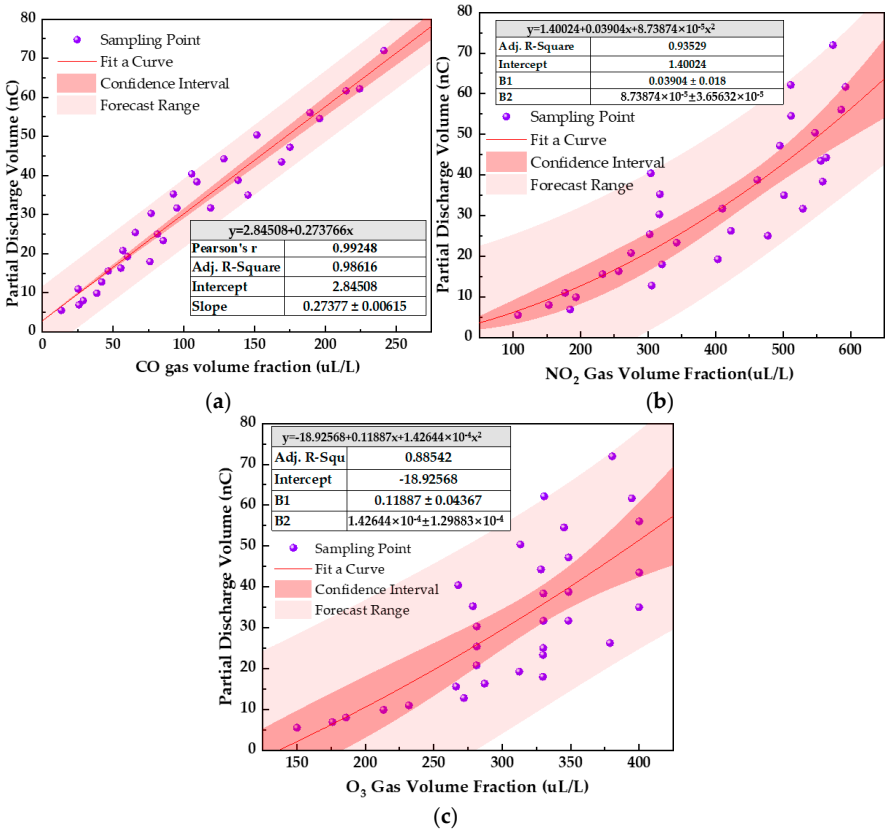


Figure 11. Fitted curves of CO, NO_2, and O_3 volume fractions versus partial discharge volume in Metal Protrusion Discharge. (**a**) CO gas volume fraction fitting curve, (**b**) NO_2 gas volume fraction fitting curve, (**c**) O_3 gas volume fraction fitting curve.

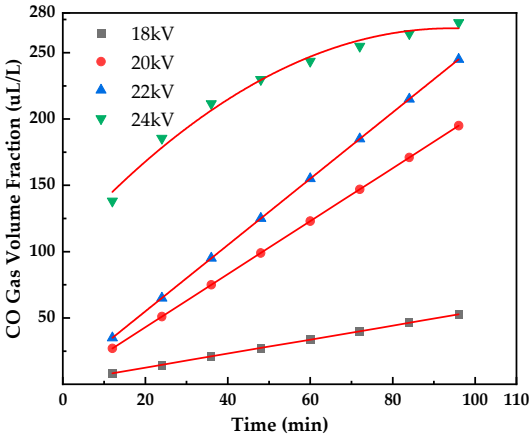


Figure 12. Variation curve of volume fraction of CO.

(2) Volume Fraction Change Characteristics of NO_2

The volume fraction of NO_2 gas change curve is shown in Figure 13. With the increase of discharge time, the gas ionization degree grows, and the NO_2 gas volume fraction has a tendency to grow. In addition, the growth trend of NO_2 gas volume fraction is affected

by the voltage level. The higher the voltage level, the greater the degree of ionization of the gas in the discharge interval, and the volume fraction of NO_2 gas will also increase. The volume fraction of the NO_2 gas curve first grows linearly, and then there is a tendency for saturation.

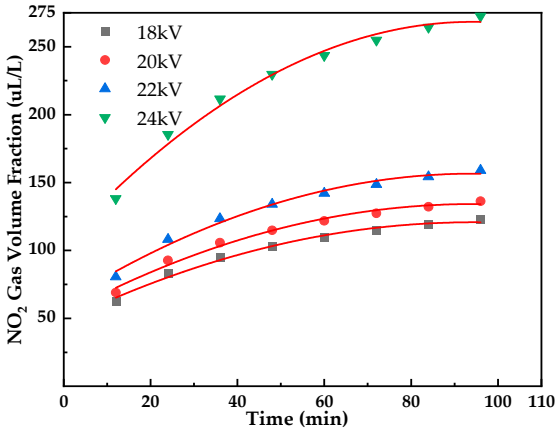


Figure 13. Variation curve of volume fraction of NO_2.

(3) Volume Fraction Change Characteristics of O_3

The volume fraction change curve of O_3 gas is shown in Figure 14. With the increase of discharge time, the ionization degree of gas grows, and the volume fraction of O_3 gas has a tendency to grow. In addition, the growth trend of the volume fraction of O_3 gas is also affected by the voltage level. The higher the voltage level, the greater the degree of ionization of the gas in the discharge interval, the volume fraction of O_3 gas will also increase. The volume fraction curve of O_3 gas first grows linearly, and then has a saturation trend.

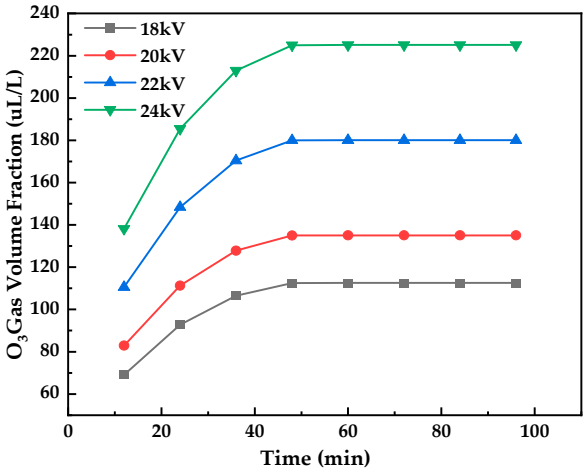


Figure 14. Variation curve of volume fraction of O_3.

4.2.2. Relationship Between Characteristic Gases and Discharge Volume in Gap Discharge

The curves of the gas volume fractions of CO, NO_2, and O_3 as a function of the partial discharge are shown in Figure 15. As the partial discharge time is prolonged, the CO, NO_2, and O_3 gas volume fractions all increase with the increase of the partial discharge. Insulation layer air gap defects have a uniform electric field in the discharge region compared to metal protrusion defects, and therefore require higher voltages and higher electric field strengths to force the gases to appear to breakdown. The number of

charged particles excited during the partial discharge of this kind of defects has a good correspondence with the new substances generated in the chemical reaction.

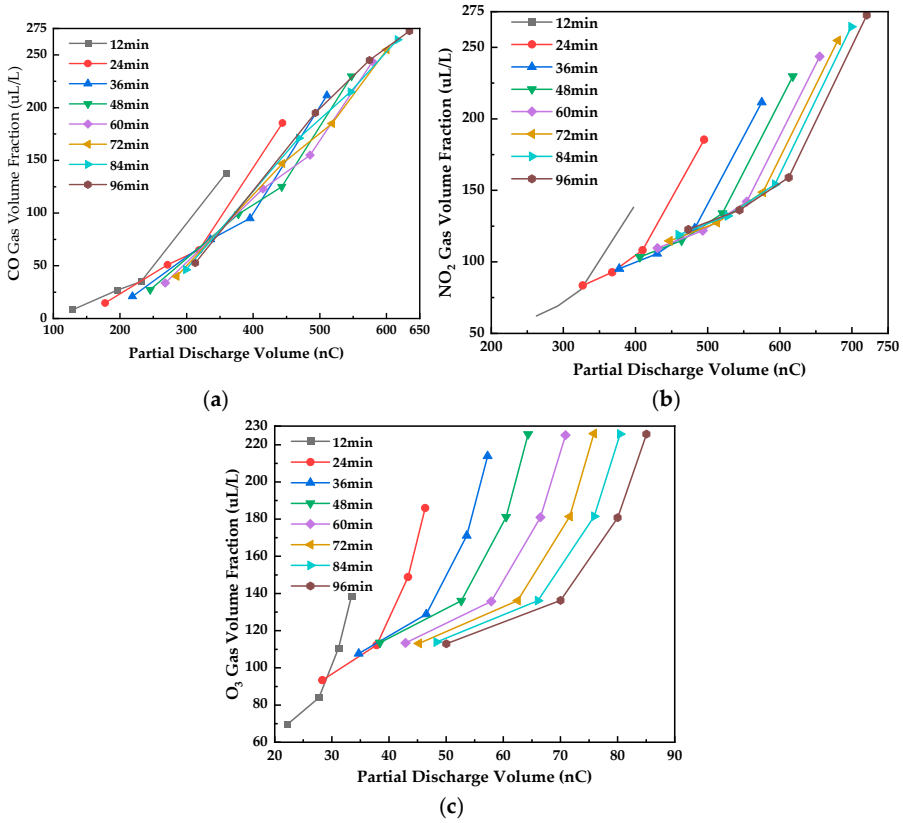


Figure 15. Variation curves of gas volume fractions of CO, NO_2, and O_3 with partial discharge volume caused by the gap. (**a**) Variation curve of CO volume fraction with partial discharge volume. (**b**) Variation curve of NO_2 volume fraction with partial discharge volume. (**c**) Variation curve of O_3 volume fraction with partial discharge volume.

4.2.3. Regression Equation of Characteristic Gas Volume Fraction and Discharge Volume in Gap Discharge

The fitted curves between the volume fractions of CO, NO_2, and O_3 gases and the partial discharges under the gas gap defects were similarly calculated using the previous regression equation. The obtained regression equations for the volume fractions of CO, NO_2, and O_3 are shown in the following equation.

$$y = -1.09501e^{-4}x_{CO}^2 + 0.16575x_{CO} + 25.34641 \quad (9)$$

$$y = -0.00164x_{NO_2}^2 + 0.79207x_{NO_2} - 20.37644 \quad (10)$$

$$y = -0.00308x_{O_3}^2 + 2.49203x_{O_3} + 26.78764 \quad (11)$$

where x_{CO}, x_{NO_2}, x_{O_3} represent the volume fractions of CO, NO_2, and O_3 when the partial discharge is y. The regression equation, 95% confidence interval, and 95% prediction space for partial discharge volume are plotted as in Figure 16.

4.3. Characterization of Characteristic Gases Generated by Metal Particle Discharge

During the manufacturing, transportation, operation, and maintenance of switchgear cabinets, complex industrial control factors cause tiny metal particles to appear in the cavities. During normal operation of the air switchgear, tiny metal particles jump, and this movement changes with the continuous alteration of the working voltage phase. This variation results in a highly unstable partial discharge, thereby augmenting the complexity of

research. The size, shape, material, and quantity of metal particles inside the switchgear can affect the generation of partial discharge. However, the number of metal particles inside the switchgear has the greatest impact on partial discharge. At the same time, for the convenience of experiments, this paper uses the number of free metal particles as the test variable to study the effect of the number of metal particles on partial discharge. The volume fraction data of the characteristic gases under different discharge durations with the number of free metal particles as a test variable are shown in Table 1.

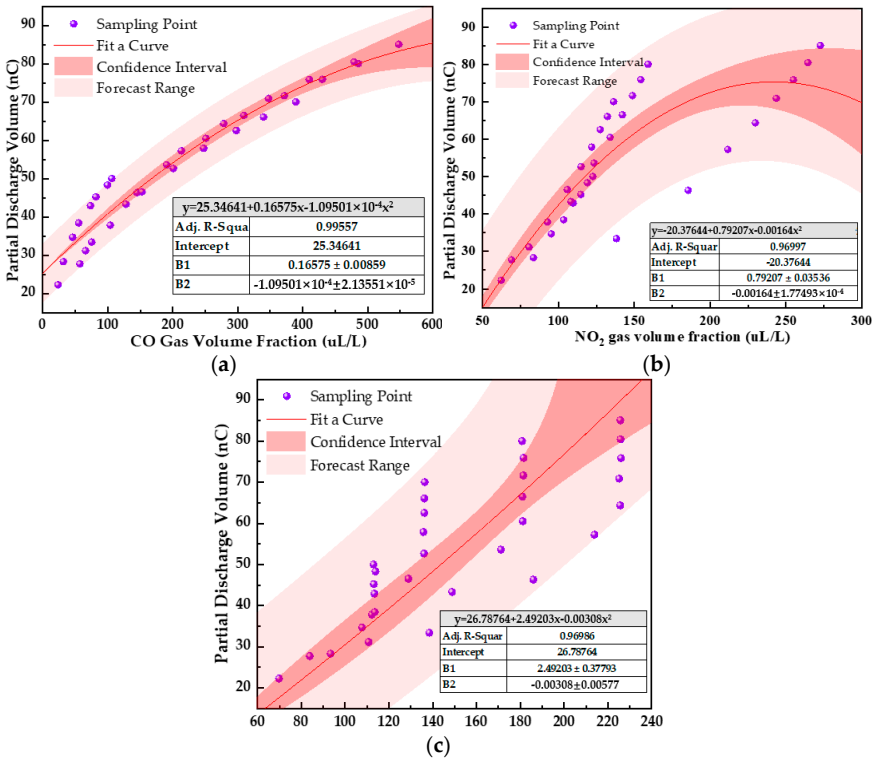


Figure 16. Fitted curves of CO, NO_2, and O_3 volume fractions versus partial discharge volume in Gap Discharge. (**a**) CO gas volume fraction fitting curve. (**b**) NO_2 gas volume fraction fitting curve. (**c**) O_3 gas volume fraction fitting curve.

Table 1. Data table of volume fractions of gases characterized by metal particle defects.

Discharge Time (min)	Q (nC)	CO (uL/L)	NO_2 (uL/L)	O_3 (uL/L)
50 Particles				
40	3	6	58	98
80	4.1	7.5	70	110
120	4.8	8	98	121
100 particles				
40	4	7	60	105
80	4.9	10	75	120
120	5	13.5	101	128
150 particles				
40	5	13	80	115
80	5.8	14	105	128
120	6.1	18	131	135
200 particles				
40	5.5	13.4	106	120
80	6.4	24	143	140
120	7	26	180	145

In the four experiments of 50, 100, 150, and 200 metal particles, the volume fractions of CO, NO_2, and O_3 were not high due to the discontinuous discharge process of metal particle defects. Due to its strong oxidizing properties, O_3 is prone to undergo redox reactions with other components in the air and easily oxidized substances in the insulation layer, thus reducing its impact on CO and NO_2. This results in a higher volume fraction of NO_2 gas. Mathematical fitting was performed on the data in Table 1, and the fitting curve is shown in Figure 17. The regression equation is shown in the following equation.

$$y = -0.00648x_{CO}^2 + 0.36345x_{CO} + 1.68393 \quad (12)$$

$$y = -1.58597e^{-4}x_{NO_2}^2 + 0.06479x_{NO_2} + 0.41323 \quad (13)$$

$$y = 0.07653x_{O_3} - 4.20924 \quad (14)$$

where x_{CO}, x_{NO_2}, x_{O_3} represent the volume fractions of CO, NO_2, and O_3 when the partial discharge is y.

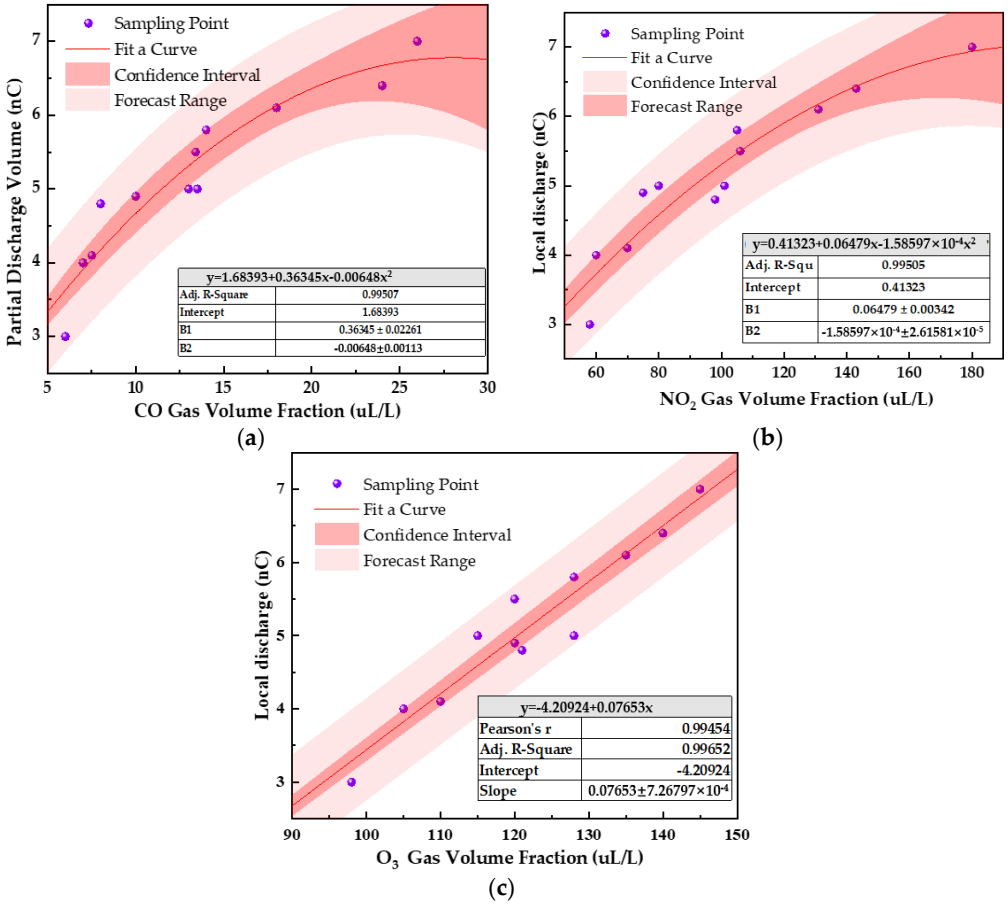


Figure 17. Fitted curves of CO, NO_2, and O_3 volume fractions versus partial discharge volume in Metal Particle Discharge. (**a**) CO gas volume fraction fitting curve. (**b**) NO_2 gas volume fraction fitting curve. (**c**) O_3 gas volume fraction fitting curve.

4.4. Inversion of Partial Discharge by Characteristic Gas Volume Fraction

Through the previous analysis, it can be found that different discharge types correspond to different gas volume fraction change rates of characteristic gases, which are unique. Therefore, this paper uses the change rate of a characteristic gas volume fraction to select the regression equation to invert the partial discharge of defect propagation in discharge. Use gas sensors to detect the volume fraction changes of characteristic gases O_3, CO, and NO_2, and then calculate the current partial discharge of the air switch equipment

based on the inversion method designed in the previous section. The calculation process of partial discharge characteristic gas inversion can be summarized as shown in Figure 18. The detection of internal insulation defects in switchgear can be achieved through online monitoring based on characteristic gases according to this process.

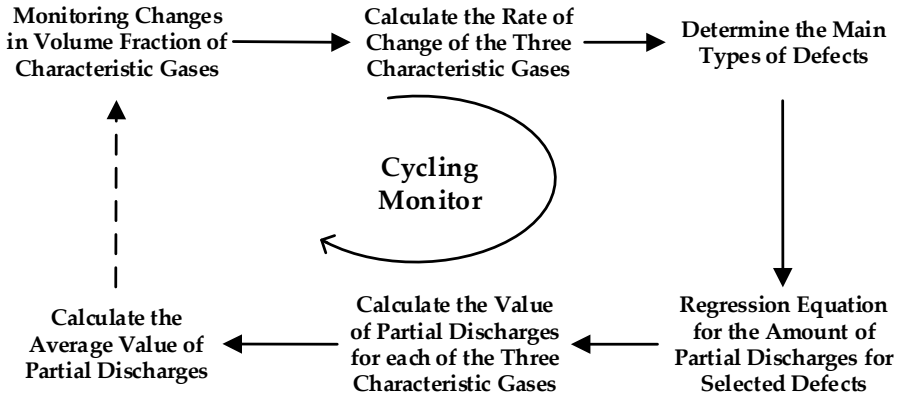


Figure 18. Flowchart of inverse partial discharge volume calculation.

The equations for calculating the first-order and second-order derivatives of the characteristic gases are shown in the following equations:

$$C_i' = \frac{C_i^{t+1} - C_i^t}{\Delta t} \tag{15}$$

$$C_i'' = \frac{C_i^{t+2} - 2C_i^{t+1} + C_i^t}{\Delta t^2} \tag{16}$$

where denotes the volume fraction of the ith characteristic gas in the layer at time t, C_i^{t+1} denotes the volume fraction of the ith characteristic gas in the layer at time $t + 1$, and C_i^{t+2} denotes the volume fraction of the ith characteristic gas in the layer at time $t + 2$.

The time-domain regression equation for the characteristic gas under the defects of metallic protrusions is shown in the following equation. Here, this paper only provides regression equations for four voltages: 11 kV, 13 kV, 15 kV, and 17 kV. However, the method proposed in this paper can fully re-estimate the situation for other voltages.

$$y_{CO} = \begin{cases} -0.0014t^2 + 1.2191t - 0.4938 & R^2 = 0.99 \quad 11\ \text{kV} \\ 0.0009t^2 + 1.3635t + 9.7560 & R^2 = 0.99 \quad 13\ \text{kV} \\ -0.0179t^2 + 2.5341t - 2.3939 & R^2 = 0.99 \quad 15\ \text{kV} \\ -0.0089t^2 + 3.3238t + 1.1509 & R^2 = 0.99 \quad 17\ \text{kV} \end{cases} \tag{17}$$

$$y_{NO_2} = \begin{cases} -0.0480t^2 + 7.5267t + 23.9337 & R^2 = 0.99 \\ -0.0797t^2 + 12.9247t + 41.0222 & R^2 = 0.99 \\ -0.0601t^2 + 10.7539t + 32.8268 & R^2 = 0.99 \\ -0.0840t^2 + 13.5991t + 42.3192 & R^2 = 0.99 \end{cases} \tag{18}$$

$$y_{O_3} = \begin{cases} -0.0301t^2 + 4.0320t + 74.5742 & R^2 = 0.998 \\ -0.0497t^2 + 6.6555t + 122.2203 & R^2 = 0.998 \\ -0.0526t^2 + 7.0292t + 129.0536 & R^2 = 0.998 \\ -0.0602t^2 + 8.0500t + 148.5663 & R^2 = 0.998 \end{cases} \tag{19}$$

The time-domain regression equation for the characteristic gas under air gap defects is shown in the following equation. Air gap discharge requires higher voltage. Here,

this paper only provides regression equations for four voltages: 18 kV, 29 kV, 22 kV, and 24 kV. The method proposed in this paper can also be used to re-estimate the situation at other voltages.

$$y_{CO} = \begin{cases} 0.0005t^2 + 0.9834t + 9.7644 & R^2 = 0.99 & 18\ \text{kV} \\ -0.0011t^2 + 4.0732t + 7.6492 & R^2 = 0.99 & 20\ \text{kV} \\ -0.0030t^2 + 5.3297t + 2.1726 & R^2 = 0.99 & 22\ \text{kV} \\ -0.0006t^2 + 5.6624t + 8.5664 & R^2 = 0.99 & 24\ \text{kV} \end{cases} \tag{20}$$

$$y_{NO_2} = \begin{cases} -0.0480t^2 + 7.5267t + 23.9337 & R^2 = 0.99 \\ -0.0797t^2 + 12.9247t + 41.0222 & R^2 = 0.99 \\ -0.0601t^2 + 10.7539t + 32.8268 & R^2 = 0.99 \\ -0.0840t^2 + 13.5991t + 42.3192 & R^2 = 0.99 \end{cases} \tag{21}$$

$$y_{O_3} = \begin{cases} -0.0128t^2 + 1.8022t + 54.5239 & R^2 = 0.998 \\ -0.0151t^2 + 2.1303t + 65.9631 & R^2 = 0.998 \\ -0.0206t^2 + 2.8987t + 86.0326 & R^2 = 0.998 \\ -0.0253t^2 + 3.5747t + 108.3213 & R^2 = 0.998 \end{cases} \tag{22}$$

The time-domain regression equation for the characteristic gas under metallic particulate defects is shown in the following equation:

$$y_{CO} = \begin{cases} -0.3608t^2 + 3.9250t - 2.5281 & R^2 = 0.99 & 50\ Grain \\ 31.6667t^2 - 278.5t + 614.3333 & R^2 = 0.99 & 100\ Grain \\ 10.9840t^2 - 117.3864t + 325.31 & R^2 = 0.99 & 150\ Grain \\ -5.6296t^2 + 78.7704t - 249.54 & R^2 = 0.99 & 200\ Grain \end{cases} \tag{23}$$

$$y_{NO_2} = \begin{cases} 16.1616t^2 - 103.8384t + 224.0606 & R^2 = 0.99 \\ 243.3333t^2 - 21491t + 4762.6667 & R^2 = 0.99 \\ 50.3788t^2 - 512.8410t + 1384.7300 & R^2 = 0.99 \\ 13.7037t^2 - 121.9630t + 362.2593 & R^2 = 0.99 \end{cases} \tag{24}$$

$$y_{O_3} = \begin{cases} 2.6696t^2 - 8.0447t + 98.1082 & R^2 = 0.998 \\ 63.3333t^2 - 547t + 1279.6667 & R^2 = 0.998 \\ 6.4394t^2 - 53.2955t + 220.4924 & R^2 = 0.998 \\ -9.2593t^2 + 132.4074t - 328.1480 & R^2 = 0.998 \end{cases} \tag{25}$$

After determining the main types of discharge defects, the volume fractions of the characteristic gases are used to calculate the corresponding partial discharges of the three characteristic gases according to the partial discharge regression equation. The reason for the calculation results of partial discharge of three characteristic gases not being equal is due to deviations in detection accuracy and the selection of regression equations, as well as the fact that partial discharge under working conditions is not a single insulation defect. Hence, it is necessary to average the calculated partial discharges. For voltage levels and metal particle quantities not considered in this paper, the expression for the characteristic gas production rate of partial discharge in switchgear can be re-estimated using the inversion method proposed in this paper.

5. Conclusions

This paper mainly studies how to detect partial discharge caused by insulation defects in high-voltage air switchgear online through characteristic gases. Three defect simulation models are constructed, and the effectiveness of the simulation models was verified using the output characteristic curves of the constructed physical defect models. After simulating the relationship between partial discharge and characteristic gas volume fraction, the inverse relationship between the change of characteristic gas volume fraction and the development of partial discharge was established. The conclusions obtained from this process are as follows:

(1) By comparing the volt-ampere characteristic curves and numerical models of partial discharge caused by insulation defects in the air switchgear on the experimental platform, it is proved that the numerical model established in this paper can describe the physical process of partial discharge in the air switchgear under atmospheric pressure;

(2) This paper establishes the correlation between the volume fraction of the characteristic gases and the partial discharge quantity. Through the volume fraction curve and the partial discharge quantity curve, it shows that CO, NO_2, and O_3 as characteristic gases have uniqueness, which can be used as the monitoring index for the study of the partial discharge quantity of insulation defects of the air switchgear cabinet.

(3) When partial discharge occurs in the air switchgear cabinet, according to the change of volume fractions of the three characteristic gases in the air components, combined with the time domain regression equation, the main type of defects in which the discharge occurs can be determined. Then, the partial discharge amount can be calculated by using the partial discharge amount inversion regression equation to calculate the partial discharge amount of the insulation defects in the air switchgear cabinet at present. This paper provides guidance for online detection of partial discharge in high-voltage air switchgear through characteristic gases.

Considering the computational complexity and feasibility, this paper adopts one-dimensional fluid mechanics to systematically analyze and study the physical process of particles at the moment of discharge in the simulation model. However, in actual working conditions, the environment where insulation defects are located is complex. Therefore, setting more variables and chemical reaction processes can obtain more accurate data results and reduce the error between simulation results and actual situations. This paper lays the foundation for the systematic study of the decomposition phenomenon under the action of discharge faults in air switchgear, and the subsequent work should focus on:

(1) The influence of air humidity, the distance between the needle plates of solid metal protrusions, and the use of different materials for each defect model on the decomposition components of air partial discharges, so as to improve the diagnostic methods of air decomposition components for the types of local discharges.

(2) Improve the decomposition components of insulator air gap discharge, metal particle discharge and metal protrusion discharge under the solid switchgear.

(3) Study the use of characteristic gases generated by insulation defect discharge to invert and calculate the partial discharge caused by defects under complex working conditions with multiple insulation defects present simultaneously.

Author Contributions: Conceptualization and writing—original draft, Y.T.; formal analysis and formal analysis and writing—review and editing, H.N. and S.W.; software, G.Z.; investigation, Y.T.; resources and writing—review and editing, H.N.; All authors have read and agreed to the published version of the manuscript.

Funding: This work is supported by the China Postdoctoral Science Foundation Project 2019M653631, National Key Research and Development Plan of China Project 2017YFB0902705, Key R&D plan

of Shaanxi Project 2024GX-ZDCYL-01-07 and 2020ZDLGY09-10, and Xi'an Science and Technology Project 22GXFW0039.

Institutional Review Board Statement: Not applicable.

Informed Consent Statement: Not applicable.

Data Availability Statement: The original contributions presented in the study are included in the article. Further inquiries can be directed to the corresponding author.

Conflicts of Interest: The authors declare no conflicts of interest.

References

1. Yan, J.; Wang, Y.; Zhou, Y.; Wang, J.; Geng, Y. A novel meta-learning network for partial discharge source localization in gas-insulated switchgear via digital twin. *IET Gener. Transm. Distrib.* **2024**, *18*, 1785–1794. [CrossRef]
2. Cairns, W.R.; Butler, O.T.; Cavoura, O.; Davidson, C.M.; Todolí-Torró, J.L.; von der Au, M. Research on environmentally friendly insulating gases under the control of PFAS and fluorine-containing gases and the prospect of application to power equipment. *Chin. J. Electr. Eng.* **2024**, *44*, 362–377.
3. Qian, H.; Zeng, X.; Zhou, K.; Zhang, W. Analysis of the correlation between GIS partial discharge current waveform and charge quantity with UHF signals. *J. Phys. Conf. Ser.* **2024**, *2757*, 012015. [CrossRef]
4. Chelmiah, T.E.; Madigan, D.C.; Kavanagh, F.D. An acoustic sensor array approach for localising partial discharges in electric machines. *Mech. Syst. Signal Process.* **2024**, *214*, 111354. [CrossRef]
5. Mier, C.; Mor, A.R.; Luo, T.; Vaessen, P. Partial discharge and interference discrimination in gas-insulated systems using electric and magnetic sensors. *Int. J. Electr. Power Energy Syst.* **2024**, *158*, 109911. [CrossRef]
6. Wang, X.; Liu, M.; Lu, F. A spaceborne broadband circularly polarized conformal antenna for UHF band applications. *Microw. Opt. Technol. Lett.* **2024**, *66*, e34115. [CrossRef]
7. Shen, C.; Yan, L. Recent development of hydrodynamic modeling in heavy-ion collisions. *Nucl. Sci. Tech.* **2020**, *31*, 90–123. [CrossRef]
8. Jiahao, S.; Shuyan, P.; JinZhao, D. Research status of partial discharge detection of power transformer based on pulse current method. *J. Phys. Conf. Ser.* **2022**, *2195*, 012024.
9. Chai, H.; Phung, B.T.; Mitchell, S. Application of UHF sensors in power system equipment for partial discharge detection: A review. *Sensors* **2019**, *19*, 1029. [CrossRef]
10. Azam, S.K.; Othman, M.; Illias, H.A.; Latef, T.A.; Fahmi, D.; Raymond, W.J.K.; Ababneh, A. Unknown PD distinction in HVAC/HVDC by antenna-sensor with pulse sequence analysis. *Alex. Eng. J.* **2024**, *91*, 457–471. [CrossRef]
11. Dukanac, Đ. Power Transformer Numerical Modeling to Locate Partial Discharge Source Using the UHF Technique. *B&H Electr. Eng.* **2023**, *17*, 24–31.
12. Yan, X.; Cheng, C.; Zhang, C.; Bai, L.; Zhang, W. On-Line Partial Discharge Monitoring System for Switchgears Based on the Detection of UHF Signals. *Appl. Sci.* **2023**, *13*, 11850. [CrossRef]
13. Mier, C.; Mor, A.R.; Vaessen, P. A directional coupler for partial discharge measurements in gas-insulated substations. *Measurement* **2024**, *225*, 113996. [CrossRef]
14. Escurra, C.M.; Khamlichi, A.; Dalstein, M.; Vidal, J.R.; Garnacho, F.; Mor, A.R.; Vu-Cong, T. Methods for partial discharge calibration in gas-insulated substations for HVDC power grids and charge evaluation uncertainty. *IEEE Sens. J.* **2023**, *23*, 23486–23493. [CrossRef]
15. Stanescu, D.; Digulescu, A.; Ioana, C.; Serbanescu, A. On the existing and new potential methods for Partial Discharge source monitoring in electrical power grids. In *Smart Trends in Computing and Communications: Proceedings of SmartCom 2021*; Springer: Singapore, 2021; pp. 155–166.
16. Stanescu, D.; Enache, F.; Popescu, F. Smart Non-Intrusive Appliance Load-Monitoring System Based on Phase Diagram Analysis. *Smart Cities* **2024**, *7*, 1936–1949. [CrossRef]
17. Jiang, J.; Wang, K.; Zhang, C.; Chen, M.; Zheng, H.; Albarracín, R. Improving the error of time differences of arrival on partial discharges measurement in gas-insulated switchgear. *Sensors* **2018**, *18*, 4078. [CrossRef]
18. Bas-Calopa, P.; Riba, J.R.; Moreno-Eguilaz, M. Measurement of corona discharges under variable geometry, frequency and pressure environment. *Sensors* **2022**, *22*, 1856. [CrossRef]
19. Zhang, X.; Gui, Y.; Zhang, Y.; Qiu, Y.; Chen, L. Influence of humidity and voltage on characteristic decomposition components under needle-plate discharge model. *IEEE Trans. Dielectr. Electr. Insul.* **2016**, *23*, 2633–2640. [CrossRef]
20. Tan, Q.; Song, B.; Wang, L.; Wu, S. Study on characteristics gases of metal protrusions partial discharge in 10-kV air-insulated switchgear. *IET Sci. Meas. Technol.* **2023**, *17*, 221–229. [CrossRef]

21. Zhu, Y.F. Modeling simulation of surface dielectric barrier discharge for nanosecond pulse of atmospheric pressure N_2-O_2 gas mixture. *High Volt. Technol.* **2013**, *39*, 1716–1723.
22. Xin, Z.; Xunnian, W. Numerical simulation and experimental verification of startup excitation characteristics of nanosecond pulsed plasma in atmospheric air. *J. Aeronaut.* **2013**, *34*, 2081–2091.

Disclaimer/Publisher's Note: The statements, opinions and data contained in all publications are solely those of the individual author(s) and contributor(s) and not of MDPI and/or the editor(s). MDPI and/or the editor(s) disclaim responsibility for any injury to people or property resulting from any ideas, methods, instructions or products referred to in the content.